metals

MDPI

Article

The Influence of High Vanadium and Phosphorus Contents on the Risk of Transverse Cracking during the Continuous Casting of Austenitic TWIP Steels

Ingrid Morel [1], Blandine Remy [1], Anne Dez [1], Barrie Mintz [2] and Colin Scott [3,*]

[1] ArcelorMittal Research, Voie Romaine-BP30320, 57583 Maizières-lès-Metz, France
[2] Department of Mechanical Engineering and Aeronautics, City, University of London, London EC1V 0HB, UK
[3] CanmetMATERIALS, Natural Resources Canada, 183 Longwood Road South, Hamilton, ON L8P 0A5, Canada
* Correspondence: colin.scott@nrcan-rncan.gc.ca

Abstract: There is considerable interest in improving the resistance of fully austenitic TWIP steels to hydrogen embrittlement; one potential route is to use V additions to promote hydrogen trapping by V(C,N) precipitates. This has the dual benefit of increasing the yield strength through precipitation strengthening and grain refinement. However, the effect on slab quality during continuous casting has not been determined. In this study, the hot ductility of two twinning-induced plasticity (TWIP) steels, Fe-0.6C-22Mn and Fe-0.6C-22Mn-0.2V, was examined over the temperature range 650–1200 °C. Tensile samples were taken from continuous cast 225 mm slabs and from 36 mm transfer bars. The addition of V caused the ductility trough in the temperature range 650–900 °C to deepen and widen and the lowest reduction in area (RA) recorded in the as-cast condition was 30%. This deterioration of hot ductility was due to V(C,N) precipitation. Even though the minimum RA was below the value often accepted to avoid cracking, no transverse cracking was observed in industrial trials and the surface quality was acceptable. The RA values of Fe-0.6C-22Mn were found to be very sensitive to the P level. However, this sensitivity was less evident when V was added, possibly due to P trapping by VC at austenite boundaries. No transverse cracking was observed in industrially produced slabs with P in the range examined (0.02 to 0.04 wt.% P).

Keywords: TWIP steels; hot ductility; continuous casting; transverse cracking

Citation: Morel, I.; Remy, B.; Dez, A.; Mintz, B.; Scott, C. The Influence of High Vanadium and Phosphorus Contents on the Risk of Transverse Cracking during the Continuous Casting of Austenitic TWIP Steels. *Metals* **2023**, *13*, 26. https://doi.org/10.3390/met13010026

Academic Editor: Noé Cheung

Received: 3 November 2022
Revised: 2 December 2022
Accepted: 19 December 2022
Published: 22 December 2022

1. Introduction

For more than two decades now, austenitic TWIP steels have been intensively studied by steelmakers interested in meeting the demands of the automotive sector for lightweight vehicles [1–4]. One of the difficulties faced by these remarkable alloys is that, although their ductility and ultimate tensile strength (UTS) are excellent, their room temperature yield strength (YS) can be disappointing compared with other cold-rolled advanced high strength steels (AHSS) [5]. This, together with a sensitivity to hydrogen embrittlement (HE) due to delayed fracture (DF) and/or stress corrosion cracking (SCC) after cold stamping (which is common to nearly all AHSS with UTS > 1000 MPa) has hampered their commercial development [2,6–8]. One solution for DF/SCC that has successfully been adopted by the manufacturers of high-strength martensitic fasteners is to provide hydrogen trapping sites in the matrix based on VC and V(C,N) nano-precipitates [9–11]. In addition, the concentration of elements such as P and S that are known to cause grain boundary embrittlement were minimized [12–16]. This technology is transferrable to cold-rolled and annealed TWIP steels and was extensively trialed by ArcelorMittal on a base Fe-0.6C-22Mn alloy in the years 2003–2006. The results were very encouraging, Figure 1a is a TEM extraction replica showing the uniform distribution of V(C,N) nano-precipitates obtained in industrial cold-rolled sheets.

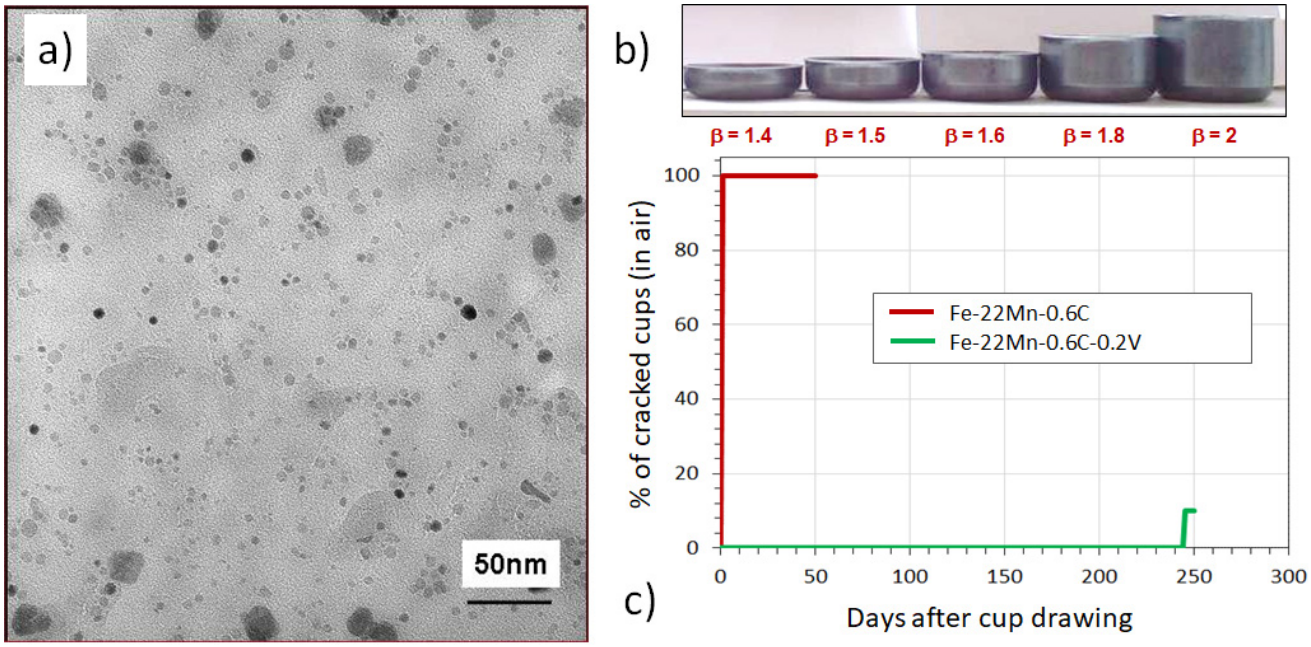

Figure 1. (**a**) TEM replica of V(C,N) in cold-rolled Fe-0.6C-22Mn-0.2V-0.01N; (**b**) deep-drawn cups used for HE testing; and (**c**) the effect on crack formation in fully drawn cups [17].

In Figure 1c, the beneficial effect of introducing V(C,N) nano-precipitates on the appearance of delayed fracture in fully drawn test cups (Figure 1b) can be seen. All of the cups made from the base Fe-0.6C-22Mn alloy cracked by DF in less than 5 days. However, with the presence of V(C,N) particles the first crack occurred after 250 days [17]. Notably, the latter was associated with a corrosion event (SCC), i.e., the V precipitates successfully eliminated DF due to *intrinsic* hydrogen, but could not entirely avoid embrittlement from *extrinsic* hydrogen (SCC). A further benefit of V(C,N) lies in the precipitation hardening and grain refining ability of this element. Previous work on cold-rolled Fe-(0.6–0.9)C-(17–22)Mn alloys [5] showed that, of the classical microalloying additions, Ti is the most efficient precipitation strengthener but that the effect saturates beyond additions of 0.1 wt.%. In the same study, Nb was found to have only a small influence on YS and V had an intermediate effect. However, V has the important advantage that there is no saturation, even with additions up to 0.9 wt.% [5,18]. Indeed, a useful increase in YS of ~150 MPa was obtained from the addition of about 0.2 wt.% V to the Fe-0.6C-22Mn-0.01N base alloy [1,5].

The industrial production of C-Mn HSLA steels has shown that low to moderate V microalloying additions generally have little negative influence on hot ductility [19,20]. Only when the V level exceeds 0.1% in some high N grades is there a risk of transverse cracking during continuous casting [20]. Concerning the effect of V on the hot ductility of high Mn austenitic steels, virtually no industrial data exist and only a few laboratory studies have been published [20–24]. One recent report on as-cast high-aluminium Fe-18%Mn-0.6%C-1.5Al TWIP steels with 0.01 wt.% N [24] examined the effect of V additions in the range 0.05 wt.% to 0.7 wt.% on hot ductility and concluded that ductility only started to suffer when the V level exceeded 0.3 wt.%. The results of that investigation are discussed elsewhere in this Special Issue [25]. A further consideration is the influence of the P content on hot ductility. Controlling P to low levels in high manganese steels is difficult and expensive, requiring the use of low P ferromanganese and/or electrolytic manganese additions. There is, therefore, a strong economic interest in ascertaining the maximum P content that can be tolerated in terms of acceptable hot ductility and on resistance to hydrogen embrittlement. The present investigation was designed to examine the influence of V and P additions on the castability of this alloy.

2. Experimental Section

All of the alloys considered here were obtained from industrial trial heats that were melted and continuously cast into 225 mm thick slabs at the ArcelorMittal Industeel Charleroi facility in Belgium. The compositions were determined using a combination of optical emission spectroscopy (OES) and LECO combustion analysis for C, N, and S contents [26], and are given in Table 1.

Table 1. The composition of the steels examined, in wt.%.

Steel	C	Mn	Si	Al	N	S	P	V
1A	0.6	22	0.2	0.002	0.01	0.001	0.027	0
2A	-	-	-	-	-	-	0.036	0
3A	-	-	-	-	-	-	0.040	0
4A	-	-	-	-	-	-	0.022	0.23
5A	-	-	-	-	-	-	0.023	0.21
6A	-	-	-	-	-	-	0.032	0.20

The base alloy composition of the steels was 0.6 wt.% C, 22 wt.% Mn, 0.2 wt.% Si, 0.01 wt.% N with very low S (0.001 wt.%) and Al ($\leq$0.005 wt.%) contents. Three of the steels examined (1A, 2A and 3A) were V-free, and three contained ~0.2 wt.% V. The other variable in the composition was the P level, varying from 0.022 wt.% to 0.040 wt.%. This range reflects the practical economic steelmaking capability of the production site for the alloy in question. The segregation levels of Mn, Si and P in one as-cast slab were studied by wavelength dispersive X-ray mapping (WDX) in a Cameca SX100 Electron Probe Micro-Analysis (EPMA) system operated at 20 kV with 1 μA beam current, a dwell time per pixel of 50 ms and a 5 μm step size. The other slabs were systematically checked for segregation levels using optical emission spectroscopy (OES). Hot ductility tests were carried out on longitudinal tensile samples taken from the as-cast 225 mm slabs and from 36 mm thick transfer bars that were cropped after the roughing stage. The slab sample tensile axis was located 15 mm below the slab surface, in the columnar growth region. The transfer bar tensile specimens were milled at one-quarter thickness—the latter are referred to as solution-treated in the text. The hot ductility tests were carried out under an argon atmosphere in a Gleeble 1500 thermo-mechanical simulator. The temperature was controlled by a thermocouple welded directly to the sample gauge region. Firstly, the specimens were heated to 1210–1240 °C at a heating rate of 50 °C s^{-1} and held for 60 s. Then, they were cooled at a rate of 10 °C s^{-1} to the test temperature, held at temperature for a stabilization time of 15 s followed by straining to failure at a strain rate of 5×10^{-3} s^{-1}. Figure 2a shows the dimensions of the hot ductility tensile specimens and Figure 2b illustrates the thermal profile used in the tests. The reduction in area at fracture (%RA) was calculated using Equation (1).

$$\%RA = (A_i - A_f)/A_i \quad (1)$$

where A_i is the initial cross-sectional area and A_f is the final cross-sectional area at the fracture surface.

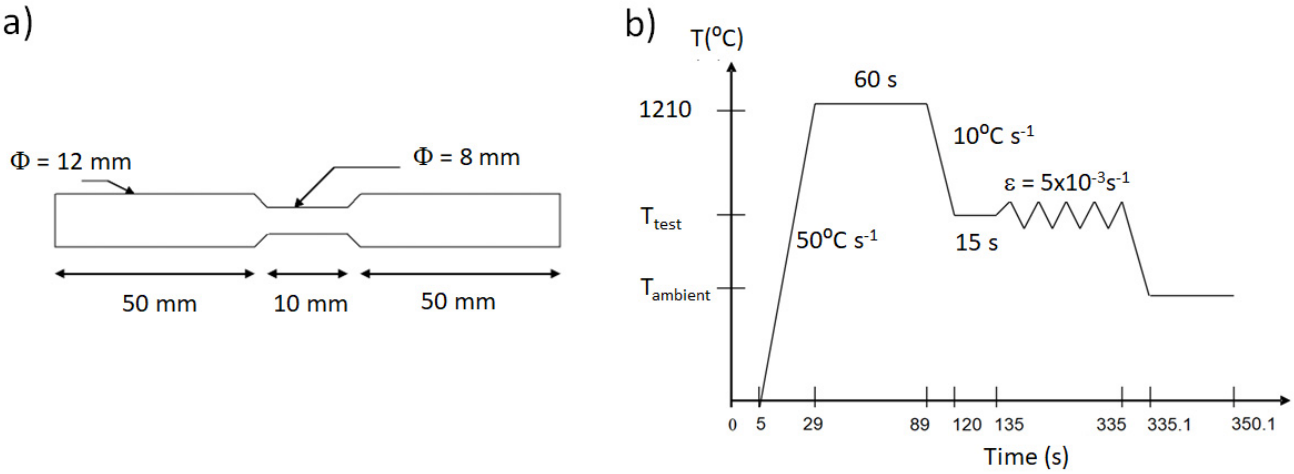

Figure 2. Schematic diagrams showing (**a**) the tensile test specimen geometry and (**b**) the thermomechanical testing cycle.

A further set of hot tensile tests was carried out using samples from laboratory cast ingots in order to study the rheology of the base material. These tests were performed with the same Gleeble 1500 simulator (Dynamic Systems Inc., Poestenkill, NY, USA) using specimens that were identical to Figure 2a, except that the gauge length was increased to 20 mm. This produced a uniform temperature zone of ~10 mm in length. The samples were deformed at a constant rate (1×10^{-2} s^{-1}) and the applied strain was estimated from the cross-head displacement, as measured by an LVDT sensor. Finally, optical microscopy was carried out using an Olympus PMG 3 microscope (Orinpasu Kabushiki-kaisha, Shinjuku, Japan) after Nital etching. Detailed microstructure and fractography observations were made using a LEO 982 FEG-SEM (Carl Zeiss AG, Oberkochen, Germany).

3. Results

The solidification structure of an as-cast slab of steel 6A can be seen in the macroscopic etch of Figure 3b. The austenite grain size was measured using the line intercept method at different depths (0.5 cm, 1 cm, and 4 cm) from the slab surface (Figure 3a). It was found that the as-cast slab grain size varied between 1 and 2 mm in the region of interest. After roughing, the austenite grain size was reduced to approximately 100 µm. Three regions corresponding to the positions of the columnar grain (C), equiaxed grain (E) and axial (A) regions were chosen for EPMA. The segregation maps obtained for Mn and P are shown in Figure 4. EPMA maps for Si show very similar segregation patterns to Mn and are therefore not shown.

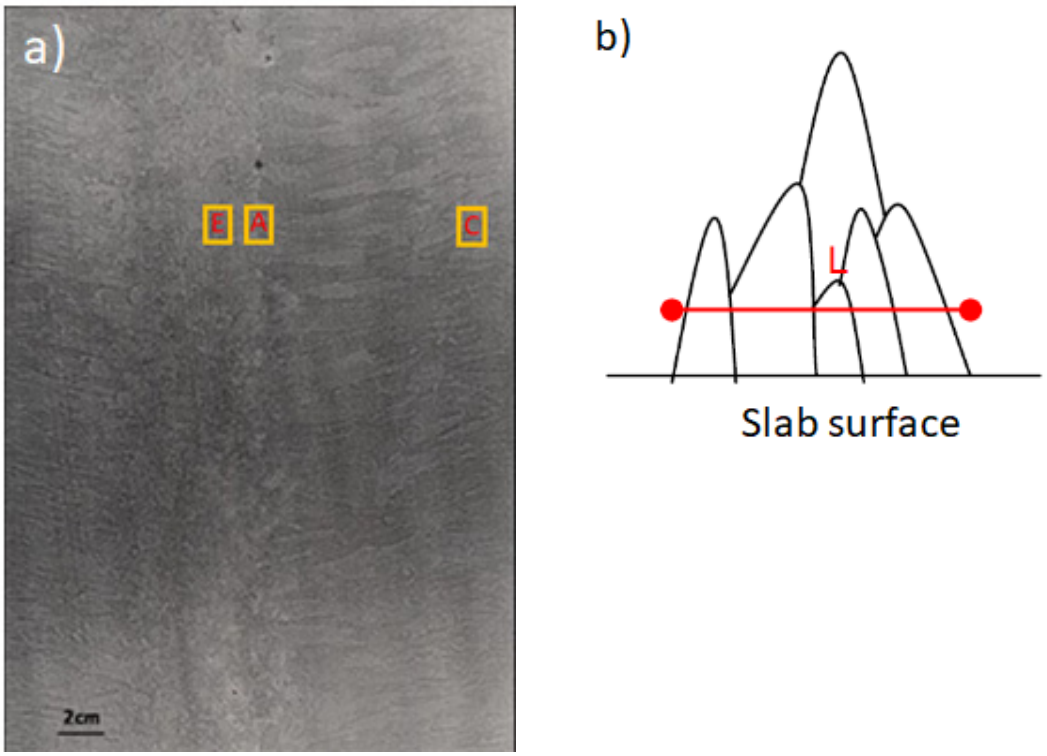

Figure 3. (**a**) Macroscopic etch of a continuous cast slab of steel 6A (containing 0.2 wt.% V and 0.032 wt.% P) showing the solidification structure and the positions of the columnar grain (C), equiaxed grain (E) and axial (A) regions chosen for EPMA, (**b**) illustration of the method used for austenite grain size measurement.

The EPMA maps for Mn, Si and P in the columnar grain region (C) show very uniform chemical distributions and no significant macro-segregation of these elements is apparent in this region. In contrast, there is significant segregation of all three elements to the interdendritic regions in both the equiaxed (E) and especially in the axial (A) regions. A total of ten regions were selected from segregated areas in the (E) [4 regions] and (A) [6 regions] maps. Each region corresponded to a square of ~100 µm × 100 µm (i.e., 400 analysis points). The average concentrations of Mn, Si and P were then obtained from each of these regions. Table 2 contains the average and peak macro-segregation ratios for Mn, Si and P from all 10 regions.

Table 2. Average and peak macro-segregation ratios in regions E (equiaxed) and A (axial).

	Mn	**Si**	**P**
Average macro-segregation ratio	1.16	1.39	2.99
Highest macro-segregation ratio	1.24	3.15	4.36

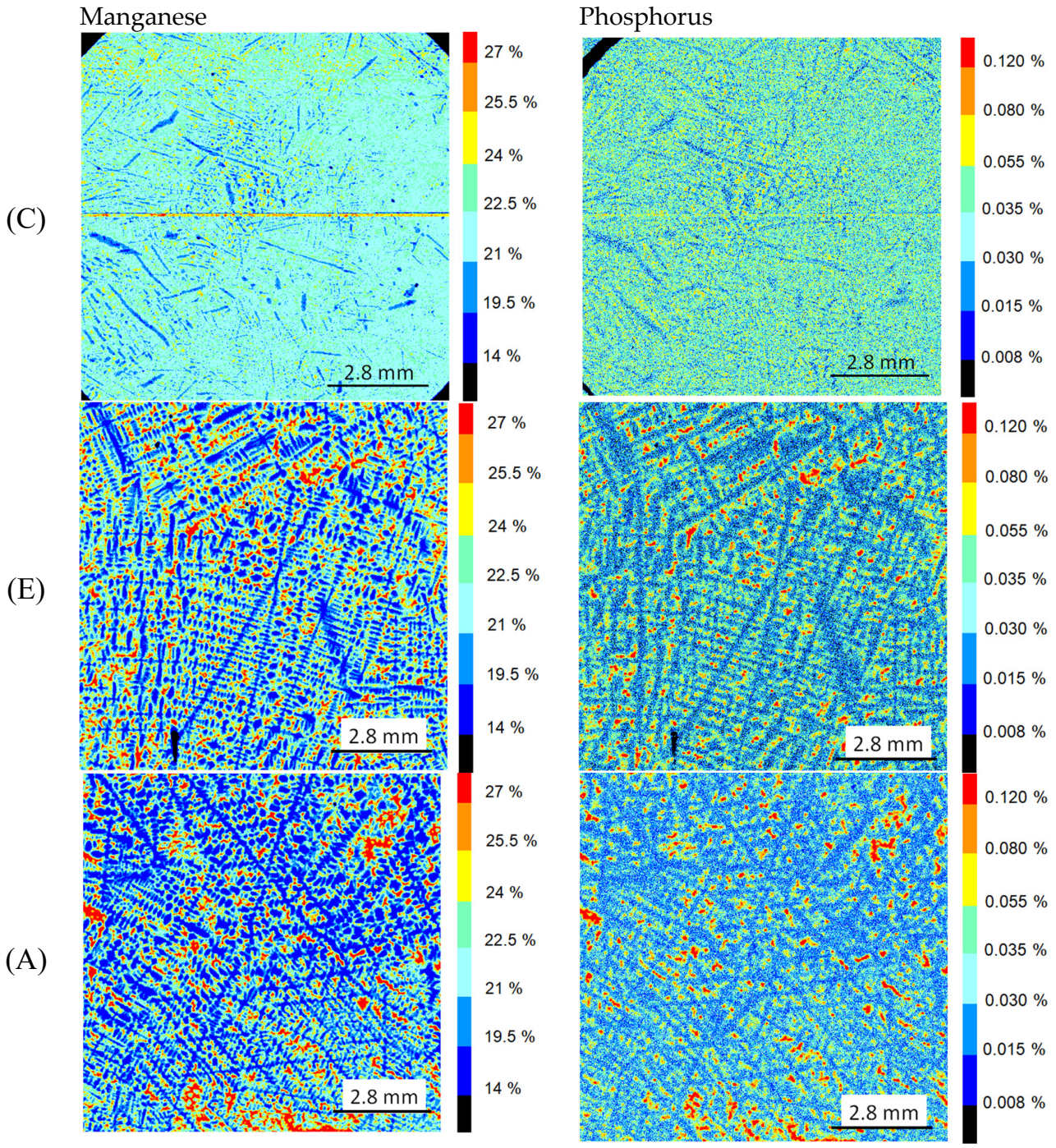

Figure 4. EPMA maps showing the distribution of Mn (**left**) and P (**right**) in the columnar grain (**top row**) equiaxed grain (**middle row**) and axial (**bottom row**) regions. The colour bars are %. wt.

Most notably, the peak segregated P content attains values of 0.13 wt.%, i.e., more than four times the nominal in these regions. No maps of C or V distributions in as-cast slabs were made. However, EPMA maps from other studies have shown that V also segregates to interdendritic regions [27]. C segregation is also significant. This element co-segregates strongly with Mn as illustrated by the transmission electron microscopy (TEM) electron energy loss spectroscopy (EELS) data [28] from a cold-rolled and annealed strip of Fe-0.7C-22Mn alloy (Figure 5).

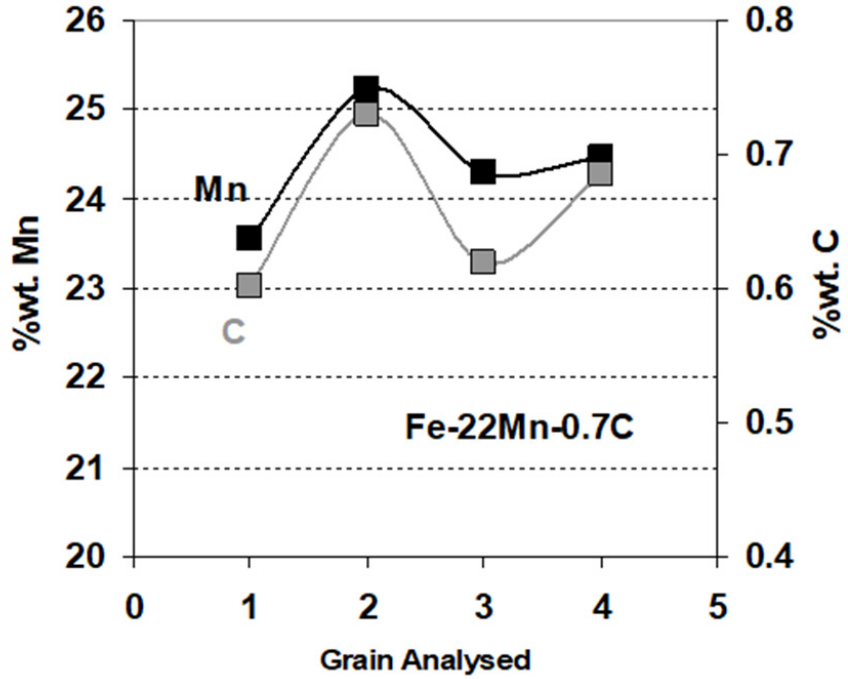

Figure 5. TEM EELS data illustrating the co-segregation of carbon with manganese in cold-rolled and annealed Fe-23Mn-0.7C [28].

For clarity, the hot ductility curves are shown in Figure 6 for a V-free steel, (1A) and a 0.2%V containing steel (4A) which had a similar P content. Both alloys were in the solution-treated condition. The V addition both deepens and widens the ductility trough.

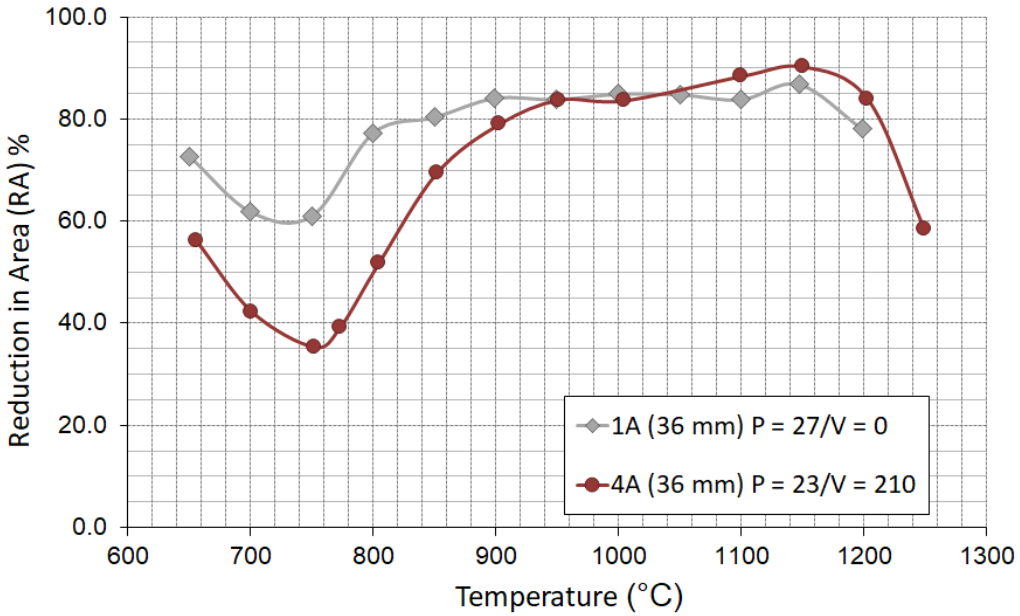

Figure 6. Hot ductility for V-free steel (1A) and a 0.2 wt.% V containing steel (4A) in the solution-treated condition.

The complete hot ductility curves for alloys 1A–6A in the solution-treated condition are shown in Figure 7. All steels showed a well-defined hot ductility trough, with a minimum that occurred in the temperature range 700–800 °C, usually close to 750 °C. For all of the P contents tested, the V-free steels (dashed lines) generally show better hot ductility than the V steels (solid lines) at temperatures below 950 °C. In the V-free alloys the minimum RA is 45%, whereas for 0.2 wt.% V containing steels, the RA values are all lower (35–43%). The

ductility curves for the V steels are quite similar and appear to be nearly independent of the P level. In contrast, the V-free steels are very sensitive to the P concentration. For these alloys, increasing the P content both deepens and widens the trough.

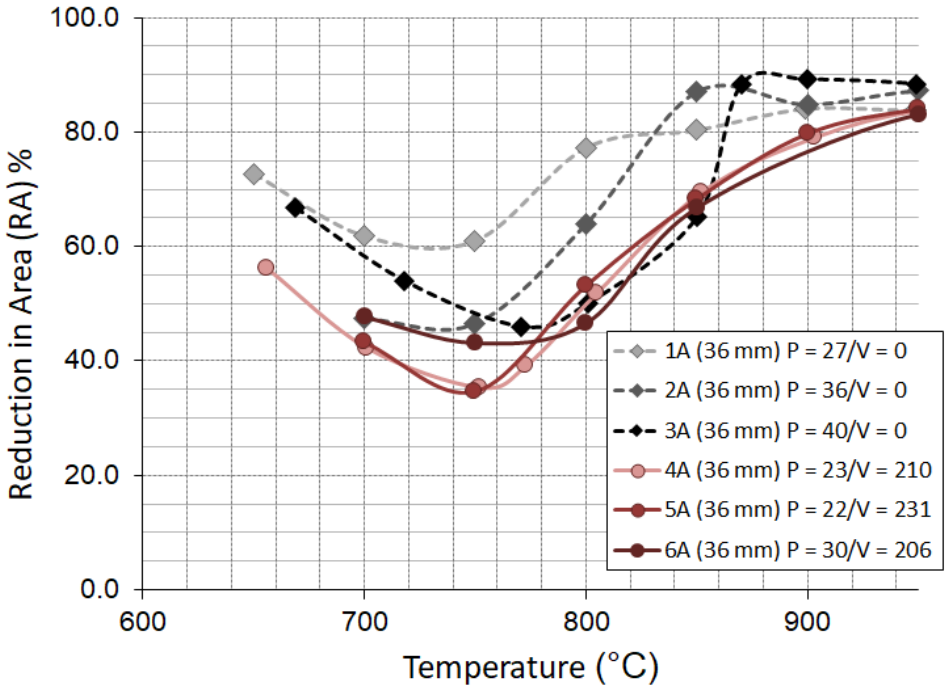

Figure 7. Hot ductility curves for the V-free steels (dashed lines) and V steels (solid lines) examined in the solution-treated condition.

The hot ductility curves for the as-cast (225 mm) state are shown in Figure 8 (dashed lines, suffix 225 mm) for selected steels 2A–4A. They are compared with the solution-treated (36 mm) condition of the same alloys (solid lines, suffix 36 mm). At higher temperatures the hot ductility curves for the as-cast state are generally much worse than for the solution-treated condition. The as-cast tensile samples were cut 15 mm below the slab surface, in the columnar grain zone (Figure 3) where the austenite grain size was greater than 1 mm. This is a factor of ~10 times greater than the solution-treated specimens so it is likely that the coarse grain size explains the poorer high temperature behaviour. The increased scatter in the as-cast data makes it difficult to draw any firm conclusions about the relative importance of the P and V contents on the ductility trough. However, it does appear that the negative effect of increasing the P concentration from 0.036 wt.% to 0.040 wt.% on the ductility minima of the V-free steels 2A and 3A is much more pronounced in the as-cast state. This is logical, if the segregation of P to austenite grain boundaries is the dominant embrittling factor.

Optical examinations of micro-sections taken next to the point of fracture of the solution-treated 0.2 wt.% V steel samples tested at a temperature close to the minimum ductility are presented in Figure 9. Figure 9a shows an image of a nital etched steel with cracks at the grain boundaries typical of grain boundary sliding and intergranular failure due to microvoid coalescence. In Figure 9b, some coarse precipitates (probably cementite formed during the final cooling step) can be seen decorating the austenite grain boundaries. This was further studied by SEM examination, (Figure 10a–c). The fracture surfaces at temperatures close to the minimum RA were a mixture of intergranular ductile with many small cavities due to microvoid coalescence and flat plane fractures due to grain boundary sliding. Fractures outside the trough (not shown) were ductile transgranular.

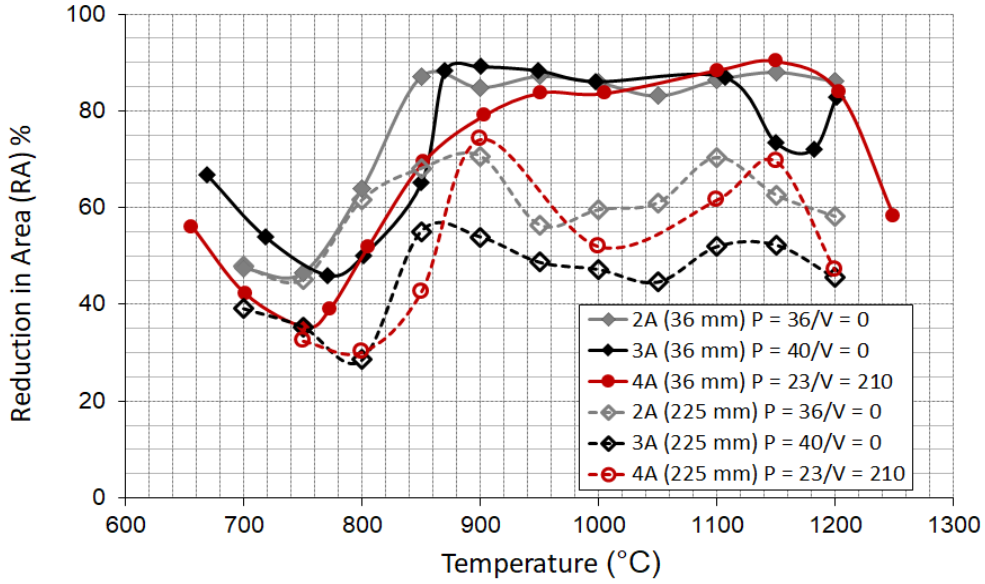

Figure 8. Hot ductility curves for selected solution-treated (solid lines) and as-cast (dashed lines) alloys.

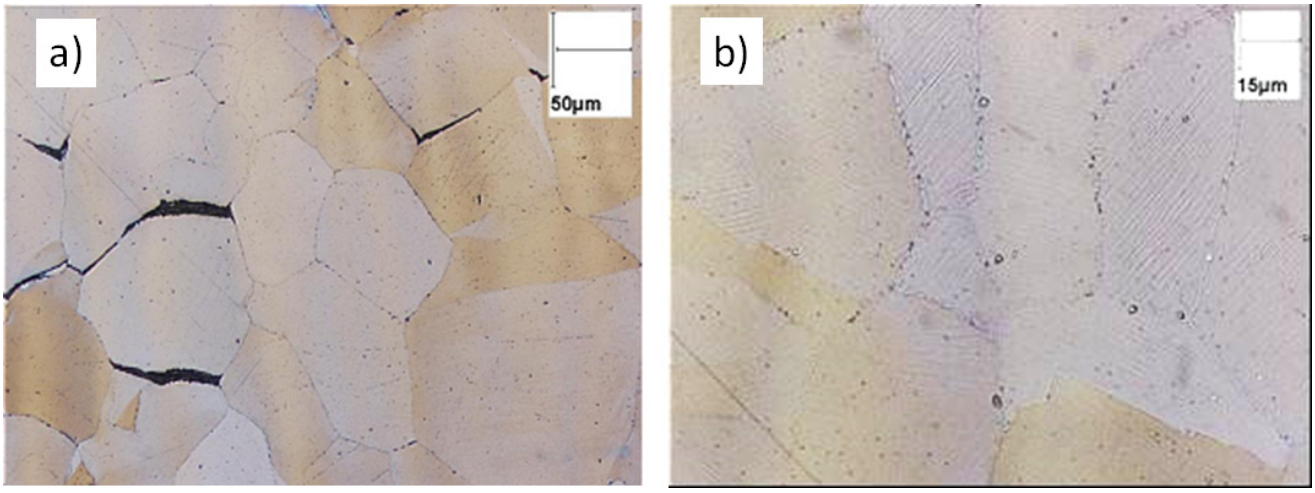

Figure 9. Optical micrographs of solution-treated 0.2 wt.% V steel after testing at 800 °C at a section close to the point of failure (**a**) showing intergranular cracking (200×) and (**b**) the presence of precipitates decorating the austenite grain boundaries (500×).

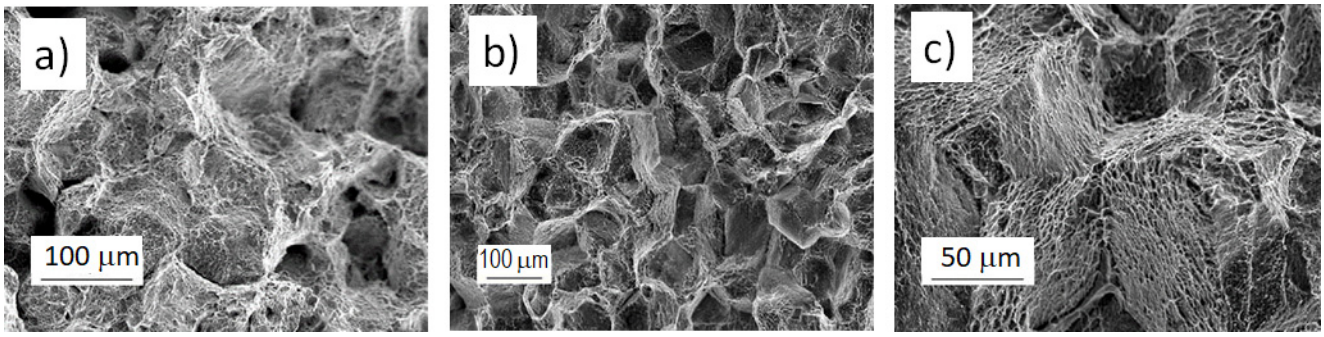

Figure 10. (**a**) Steel 3A (V-free) solution-treated and strained at 800 °C, (**b**,**c**) Steel 5A (0.21 wt.% V) solution-treated and strained at 762 °C.

A typical series of stress/elongation curves is given in Figure 11 for a laboratory ingot of Fe-22Mn-0.6C TWIP steel for temperatures in the range 800–1200 °C. The steel had no V or P and contained <20 ppm wt. Al. No evidence of dynamic recrystallisation (DRX) is seen throughout the whole temperature range 800–1200 °C

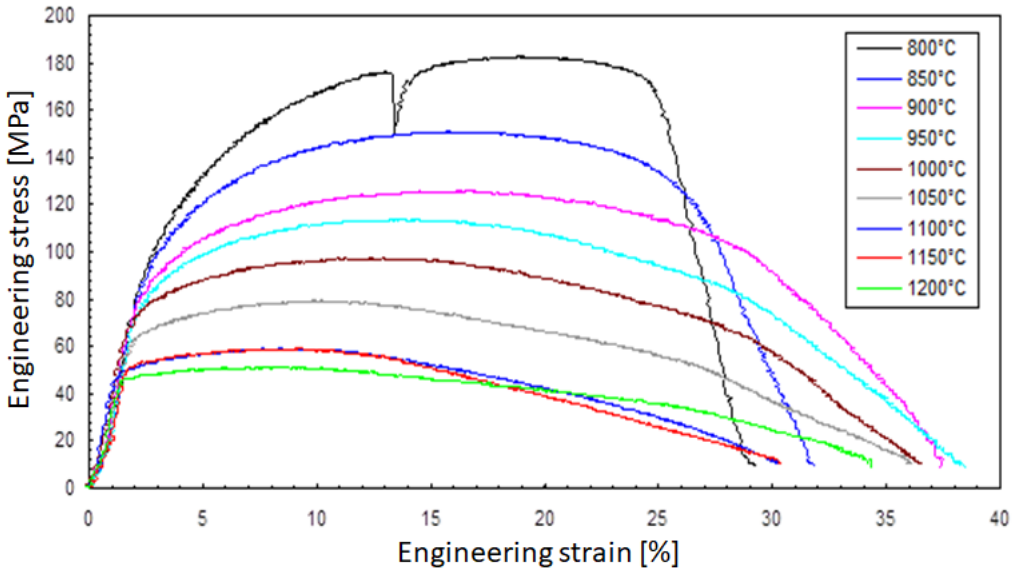

Figure 11. Stress/elongation curves for a laboratory ingot of Fe-22Mn-0.6C TWIP steel for temperatures in the range 800–1200 °C. The steel had no V or P and contained less than 20 ppm wt. of Al. The strain rate was 1×10^{-2} s^{-1}.

4. Discussion

In the steel with low P and no V (steel 1A) in Figure 6, the hot ductility is very high and only a slight trough is observed below 800 °C. Similar troughs in other fully austenitic alloys are often associated with the suppression of DRX, the precipitation of AlN, or void formation promoted by grain boundary sliding (GBS) [24,25,29]. Here, we see no evidence of DRX at any temperature (Figure 11) and the Al content is too low (20 ppm wt.) to introduce significant AlN precipitation. Cementite formation does not occur until the temperature falls below 700 °C and the allotropic phase transformation occurs even later, at just above 500 °C (see Figure 12a); therefore, it seems probable that GBS is the controlling mechanism. With the addition of V, the ductility trough deepens and widens, as shown in Figure 6. V can be present in two states in the trough region—as substitutional atoms in solid solution and as a precipitate, in particular, as VC, VN or V(C,N). Both forms can have a negative effect on hot ductility. Depending on their size, location and density, precipitates may provide an increment in yield stress, inhibit grain growth and static recrystallization, hinder DRX and dynamic recovery and promote intergranular failure by wedge cracking or void nucleation. V in solid solution may provide solid solution hardening, reduce climb and vacancy diffusion, modify transformation temperatures and retard grain growth and DRX via solute drag effects [30]. It is therefore not a simple task to identify the critical operating mechanism(s) that influence hot ductility.

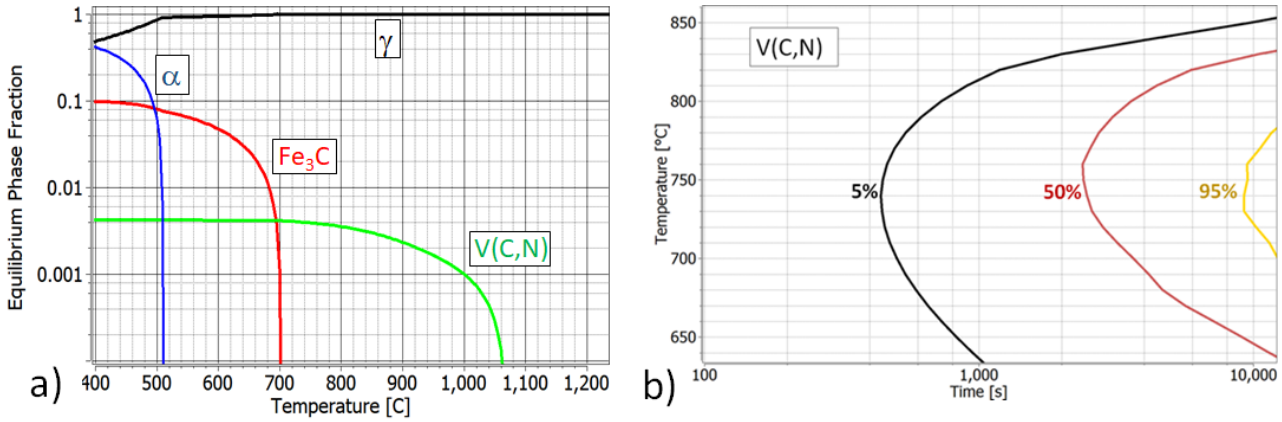

Figure 12. (**a**) Equilibrium volume fraction of V(C,N) precipitated in steel 5A as a function of temperature, (**b**) PTT calculation for V(C,N) in steel 5A assuming nucleation on dislocations with a density of 1×10^{14} m^{-2}.

Figure 12a shows the result of an equilibrium thermodynamic calculation for the evolution of the phase fractions of austenite, ferrite, cementite and V(C,N) in Steel 5A using the MatCalc 6.03 software and the mc_fe_2.059 database [31]. For this composition, V(C,N) begins to form at around 1060 °C and the maximum precipitated fraction is achieved at ~700 °C. However, equilibrium calculations do not reflect the kinetic aspects of precipitation that often dominate during steel processing. Accordingly, a full kinetic precipitation-time-temperature (PTT) calculation for V(C,N) is presented in Figure 12b. Here, the nucleation sites for precipitates were dislocations and the mean dislocation density was assumed to be 1×10^{14} m^{-2}. This is a reasonable value for the expected dislocation density in unrecovered austenite during straining at the temperatures of interest [32]. The curves represent the locus of points where a constant fraction (5%, 50% and 95%) of the total precipitated volume occurs. These C-shaped plots are limited by chemical driving force for precipitation at high temperatures and diffusion of the rate-defining element (V) at low temperatures. The calculation predicts that the first V(C,N) precipitates form after an incubation time of approximately 400 s at a temperature of 740 °C. This is actually longer than the duration of the hot tensile tests. However, the incubation time will decrease if the dislocation density is higher and/or if there are locally segregated regions where higher than nominal concentrations of V, C and N exist.

The agreement between the position of the ductility trough minima of the V steels (750 °C) and the position of the V(C,N) PTT nose at 740 °C is very good, strongly suggesting that it is V(C,N) precipitate formation that determines the ductility minimum [33]. The increase in the trough width can also be explained by Figure 12 as follows. When V is added, the onset of the ductility trough shifts from ~800 °C to ~950 °C on the high temperature side (Figure 6). This is considerably below the equilibrium solution temperature for V(C,N) precipitation in these steels (1060 °C), so some precipitate formation is possible at 950 °C (Figure 12a). However, the kinetic model (Figure 12b) shows that this is unlikely to happen in a time compatible with the duration of the hot tensile tests. The initial decrease in ductility at high temperatures is therefore likely to occur due to precipitates formed in areas where local segregation of C, V and N occurs, either in interdendritic regions or at austenite grain boundaries. These predictions are in good agreement with the experimental results of Kang et al. [24].

As the P content increases, the ductility trough of the V-free steels becomes deeper and widens at the high temperature side. This effect has been attributed to the formation of eutectic phosphide precipitates in segregated interdendritic regions below oscillation marks [34]. It is interesting to observe that the V containing alloys do not show the same sensitivity to P content. One possible reason for this is that P has been shown to segregate

to VC precipitates formed at austenite grain boundaries [35]. Thus, VC can act as a trap or sink for P and beneficially reduce the amount of P segregated to boundaries.

The effect of austenite grain size is known to be a critical parameter in hot ductility behaviour [25]. In the present study, the test samples that were solution-treated were taken from transfer bars after roughing and therefore recrystallized before tensile testing, so the austenite grain size ~40–80 μm was much finer than the as-cast condition (1000–1500 μm). This refinement in grain size leads to higher RA values throughout the entire testing range (Figure 8). The lowest RA values recorded for any of the alloys tested in the as-cast condition were 30%. This was for alloy 3A (P = 40, V = 0) and alloy 4A (P = 23, V = 210). It is usually considered that steels with minimum RA values below 40% are at risk from transverse cracking. However, industrial trials have confirmed that no transverse cracks occurred in any of the alloys studied here.

5. Conclusions

The hot ductility of TWIP steels, Fe-0.6C-22Mn and Fe-0.6C-22Mn-0.2V was examined over the temperature range 650–1200 °C. Tensile samples were taken from continuous cast 225 mm slabs and from 36 mm transfer bars that were cropped after roughing. The main conclusions are as follows:

- A shallow hot ductility trough with a minimum at ~750 °C was found to be present in the V-free Fe-22Mn-0.6C TWIP steels. An addition of 0.2 wt.% V addition caused this ductility trough to deepen and widen in the range 650–900 °C due to the precipitation of V(C,N). At temperatures > 950 °C ductility is good because precipitates are either absent or too coarse to have much influence. Below 650 °C, precipitation is too slow.
- The minimum RA in the as-cast state (30%) was below that normally associated with slab cracking during straightening. Nevertheless, data from a significant number of industrial trials confirmed that no transverse cracking actually occurred with a 0.2 wt.% V addition and that good surface quality can be obtained.
- Increasing the P content significantly reduced the hot ductility of the base Fe-22Mn-0.6C TWIP steel; however, industrial trials showed that for both the base and for the V added steels, P levels in the range 0.020 to 0.040 wt.% did not cause any transverse cracking and the surface quality remained acceptable.
- V-containing alloys do not appear to show the same sensitivity to P content. The reason for this is suggested to be related to P segregation to VC precipitates located on austenite boundaries. This would have the effect of reducing the amount of P segregated to the austenite grain boundaries themselves, thus reducing the likelihood of intergranular fracture.
- Notably, the good casting ability has only been achieved by setting very low S and Al levels. MnS inclusions in the matrix and AlN precipitation at austenite grain boundaries are thus avoided. The latter is essential to suppress intergranular failure.

Author Contributions: Conceptualization, B.M. and C.S.; methodology, I.M., B.R. and A.D.; investigation, I.M., B.R. and A.D.; formal analysis, B.M. and C.S.; writing—original draft preparation, B.M.; writing—review and editing, C.S. All authors have read and agreed to the published version of the manuscript.

Funding: This research received no external funding.

Data Availability Statement: The data are not publicly available due to commercial restrictions.

Acknowledgments: The authors would like to thank CanmetMATERIALS, ArcelorMittal Research and Vanitec for their support and permission to publish these results.

Conflicts of Interest: The authors declare no conflict of interest.

References

1. Bouaziz, O.; Allain, S.; Scott, C.P.; Cugy, P.; Barbier, D. High manganese austenitic twinning induced plasticity steels: A review of the microstructure properties relationships. *Curr. Opin. Solid State Mater. Sci.* **2011**, *15*, 141–168. [CrossRef]
2. De Cooman, B.C.; Chin, K.G.; Kim, J. High Mn TWIP steels for automotive applications. *New Trends Dev. Automot. Syst. Eng.* **2011**, *1*, 101–128.
3. Kim, S.K.; Cho, J.W.; Kwak, W.J.; Kim, G.; Kwon, O. Development of TWIP steel for Automotive Application. In Proceedings of the 3rd International Steel Conference on New Developments in Metallurgical Process Technologies, Dusseldorf, Germany, 11–15 June 2007; pp. 690–697.
4. Horvath, C.D. Advanced Steels for Lightweight Automotive Structures. In *Materials, Design and Manufacturing for Lightweight Vehicles*; Woodhead Publishing: Sawston, UK, 2021; pp. 39–45.
5. Scott, C.; Remy, B.; Collet, J.-L.; Cael, A.; Bao, C.; Danoix, F.; Malard, B.; Curfs, C. Precipitation strengthening in high manganese austenitic TWIP steels. *Int. J. Mat. Res.* **2011**, *102*, 538–549. [CrossRef]
6. So, K.H.; Kim, J.S.; Chun, Y.S.; Park, K.T.; Lee, Y.K.; Lee, C.S. Hydrogen delayed fracture properties and internal hydrogen behavior of a Fe–18Mn–1.5 Al–0.6 C TWIP steel. *ISIJ Int.* **2009**, *49*, 1952–1959. [CrossRef]
7. Park, I.J.; Jeong, K.H.; Jung, J.G.; Lee, C.S.; Lee, Y.K. The mechanism of enhanced resistance to the hydrogen delayed fracture in Al-added Fe–18Mn–0.6 C twinning-induced plasticity steels. *Int. J. Hydrog. Energy* **2012**, *37*, 9925–9932. [CrossRef]
8. Olugbade, T.O. Stress Corrosion Cracking and precipitation strengthening mechanisms in TWIP steels: Progress and prospects. *J. Corros. Rev.* **2020**, *38*, 473–488. [CrossRef]
9. Manabe, T.; Miyakoshi, Y. Development of Thermal Refining Type High Tensile Bolt. *Nippon. Steel Tech. Rep.* **2019**, *122*, 117–122.
10. Namimura, Y.; Ibaraki, N.; Urushihara, W.; Nakayama, T. Development of steels for high-strength bolts with excellent delayed fracture resistance. *Wire J. Int.* **2003**, *36*, 62–67.
11. Takahashi, J.; Kawakami, K.; Kobayashi, Y. Origin of hydrogen trapping site in vanadium carbide precipitation strengthening steel. *Acta Mater.* **2018**, *153*, 193–204. [CrossRef]
12. Mintz, B.; Tuling, A.; Delgado, A. Influence of silicon, aluminium, phosphorus and boron on hot ductility of Transformation Induced Plasticity assisted steels. *Mater. Sci. Technol.* **2003**, *19*, 1721–1726. [CrossRef]
13. Su, H.; Gunawadarna, W.D.; Tuling, A.; Mintz, B. Influence of Al and P additions on hot ductility of steels. *Mater. Sci. Technol.* **2007**, *23*, 1357–1366. [CrossRef]
14. Guo, A.M.; Wang, Y.H.; Shen, D.D.; Yuan, Z.X.; Song, S.H. Influence of phosphorus on the hot ductility of 2.25Cr1Mo steel. *Mater. Sci. Technol.* **2003**, *19*, 1553–1556. [CrossRef]
15. Kang, S.E.; Banerjee, J.R.; Mintz, B. Influence of S and AlN on hot ductility of high Al, TWIP steels. *Mater. Sci. Technol.* **2012**, *28*, 589–596. [CrossRef]
16. Osinkolu, G.A.; Tacikowski, M.; Kobylanski, A. Combined effect of AIN and sulphur on hot ductility of high purity iron-base alloys. *Mater. Sci. Technol.* **1985**, *1*, 520–525. [CrossRef]
17. Feaugas, X.; Scott, C. *Le Développement des Aciers a Très Haute Résistance*; ISTE Editions: London, UK, 2022; pp. 259–290. ISBN 978-1-78949-122-7.
18. Yen, H.-W.; Huang, M.; Scott, C.P.; Yang, J.-R. Interactions between deformation-induced defects and carbides in a vanadium-containing TWIP steel. *Scripta Mat.* **2012**, *66*, 1018–1023. [CrossRef]
19. Hannerz, N.E. Critical hot plasticity and Transverse Cracking in Continuous Slab casting with particular reference to composition. *Trans. Iron Steel Inst. Jpn.* **1985**, *25*, 149–158. [CrossRef]
20. Mintz, B.; Abushosha, R. Influence of vanadium on the hot ductility of steel, Ironmaking and steelmaking. *Ironmak. Steelmak.* **1993**, *20*, 445–452.
21. Hamada, A.S.; Karjalainen, L.P. Hot ductility behaviour of high-Mn TWIP steels. *Mat. Sci. Eng. A* **2011**, *528*, 1819–1827. [CrossRef]
22. Kang, S.E.; Tuling, A.; Banerjee, J.R.; Gunawardana, W.D.; Mintz, B. Hot ductility of TWIP steels. *Mater. Sci. Technol.* **2021**, *27*, 95–100. [CrossRef]
23. Liu, H.; Liu, J.; Wu, B.; Shen, Y.; He, Y.; Ding, H.; Su, X. Effect of Mn and Al contents on hot ductility of high alloy Fe-xMn-C-yAl austenite TWIP steels. *Mater. Sci. Eng. A* **2017**, *708*, 360–374. [CrossRef]
24. Kang, S.E.; Kang, M.H.; Mintz, B. Influence of vanadium, boron and titanium on hot ductility of high Al TWIP steels. *Mater. Sci. Technol.* **2021**, *37*, 42–58. [CrossRef]
25. Mintz, B.; Qaban, A. The Influence of Precipitation, High Levels of Al, Si, P and a Small B Addition on the Hot Ductility of TWIP and TRIP Assisted Steels: A Critical Review. *Metals* **2022**, *12*, 502. [CrossRef]
26. Morel, I.; Dez, A. *ArcelorMittal Internal Report*; IRD/AUP/2008/9177; ArcelorMittal: Luxembourg, 2008.
27. Scott, C.; Gavard, L.; DeRo, A.; Evertz, T.; Maiwald, T. *New Metallurgy for Microalloyed TRIP Steels*; KI-NA-22391-EN-S; Publications Office of the European Union: Luxembourg, 2007; pp. 1–130.
28. Scott, C. Solving problems in steel metallurgy using PEELS. In Proceedings of the ICEM-15: 15th International Congress on Electron Microscopy, Durban, South Africa, 1–6 September 2002; pp. 135–136.
29. Mintz, B.; Qaban, A. Understanding the high temperature side of the hot ductility curve for steels. *Mater. Sci. Technol.* **2021**, *37*, 237–249. [CrossRef]
30. Baker, T.N. Process, microstructure and properties of V microalloyed steels. *Mater. Sci. Technol.* **2009**, *25*, 1083–1107. [CrossRef]
31. Available online: http://www.matcalc-engineering.com/ (accessed on 29 February 2022).

32. Zurob, H.S.; Hutchinson, C.R.; Brechet, Y.; Purdy, G. Modeling recrystallization of microalloyed austenite: Effect of coupling recovery, precipitation and recrystallization. *Acta Mater.* **2002**, *50*, 3075–3092. [CrossRef]
33. Jeong, J.-Y.; Hong, D.-G.; Yim, C.-H. Deep Learning to Predict Deterioration Region of Hot Ductility in High-Mn Steel by Using the Relationship between RA Behavior and Time-Temperature-Precipitation. *Metals* **2022**, *12*, 1689. [CrossRef]
34. Harada, S.; Tanaka, S.; Misumi, H.; Mizoguchi, S.; Horiguchi, H. A Formation Mechanism of Transverse Cracks on CC Slab Surface. *Trans. ISIJ* **1990**, *30*, 310–316. [CrossRef]
35. Nako, H.; Taniguchi, G.; Zhu, S.-Q.; Ringer, S.P. Influence of grain boundary segregation on temper embrittlement of Cr-Mo heat resistant steel weld metal and quantitative analysis of the amount of segregated atoms. In Proceedings of the 5th International Symposium on Steel Science (ISSS 2017), Kyoto, Japan, 13–16 November 2017; The Iron and Steel Institute of Japan: Tokyo, Japan.